Full Paper

Evaluation of a CL-20/TATB Energetic Co-crystal

Clinton J. Chapman[a] and Lori J. Groven*[a]

Abstract: Exploration of novel energetic-energetic co-crystals has greatly increased in recent years as the need for energetic materials with improved detonation performance and reduced sensitivity continues to grow. In 2015 a CL-20/TATB co-crystal was reported and touted sensitivity and detonation properties that would make it a potential replacement for the industry standard HMX. The confirmation, reproducibility, and characterization of energetic materials are still a widely debated topic especially when the material of interest has exceptional properties. In this work, CL-20/TATB co-crystals are attempted via solvent-nonsolvent (S/NS) co-crystallization to assess the formation of a true co-crystal. The prepared crystals were characterized via scanning electron microscopy (SEM), powder x-ray diffraction (PXRD), fourier transform infrared spectroscopy (FTIR), raman spectroscopy, thermogravimetric analysis (TGA), and differential scanning calorimetry (DSC). This work reproduced S/NS cocrystallization similar to that reported in 2015, provides a solubility and thermodynamic explanation behind CL-20/TATB cocrystallization, and assesses the future viability of CL-20/TATB crystals.

Keywords: Co-crystal · CL-20 · TATB · DMSO

1 Introduction

The decline in discovery of novel energetic materials with adequate sensitivity and increased performance has led to exploration of polymer-based explosives, reduced sensitivity explosives, and cocrystallization methods. Cocrystallization is already extensively used in the pharmaceutical industry to achieve tunable properties for active pharmaceutical ingredients (APIs). Pharmaceutical use of cocrystallization has been shown to improve dissolution rate, thermal stability, and bioavailability without influencing the effectiveness of the API [1,2].

In the case of energetic materials, energetic-energetic co-crystals are often favored over materials with non-energetic additives in hopes of maintaining high energy density and performance. 2,4,6,8,10,12-Hexanitrohexaazaisowurtzitane, a polycyclic nitramine, commonly referred to as CL-20, is often found in these energetic-energetic co-crystals. CL-20 is currently the most powerful commercially available explosive, making it a major focus of cocrystallization efforts [1,3–15]. CL-20 is of great interest for applications ranging from explosives to propellants; however, it is limited by its mechanical and thermal sensitivity to detonation [1,4,16]. The excellent energetic performance of CL-20 makes cocrystallization a potential method for maintaining energetic performance while reducing overall sensitivity.

Cocrystallization efforts in the energetics field have largely been placed towards finding adequate co-formers for CL-20. Several CL-20 based co-crystals have been reported with TNT, HMX, NQ, TATB, and most recently RDX co-formers [1,4,6,8,12,15]. Although some of these co-crystals can be confirmed as true co-crystals via single crystal x-ray diffraction, most require the evaluation of other characterization techniques, such as morphological observations, various forms of spectroscopy, and powder x-ray diffraction (PXRD) to support claims of true co-crystal formation [16]. While many co-crystals have been claimed, the confirmation, reproducibility, and characterization of these materials are still up for debate [16].

1.1 Previous Synthesis of CL-20/TATB

One co-former of interest is triaminotrinitrobenzene, commonly referred to as TATB. TATB is notable due to its relatively high density, moderate energetic performance, and insensitivity [11]. A CL-20/TATB co-crystal was reportedly synthesized via solvent/non-solvent (S/NS) cocrystallization using DMSO and water at 25 °C in 2015 [12]. The material was characterized via scanning electron microscopy (SEM), Fourier transform infrared spectroscopy (FTIR), Raman spectroscopy, high performance liquid chromatography (HPLC), PXRD, thermogravimetric analysis (TGA), and differential scanning calorimetry (DSC). Xu et al. [12] reported the synthesized CL-20/TATB material exhibited a mechanical sensitivity equal to that of HMX with a greater density, 1.960 g cm^{-3}, and detonation velocity, 9127 m s^{-1}. If true,

[a] *C. J. Chapman, L. J. Groven*
Department of Chemical and Biological Engineering
South Dakota School of Mines and Technology
501 E St. Joseph St, Rapid City, SD 57701, USA
*e-mail: lori.groven@sdsmt.edu

this would make CL-20/TATB an excellent candidate for replacing the current industry standard, HMX [12]. For any new material, reproducibility of physical, chemical, and performance characteristics should be confirmed before widespread adoption.

In energetic materials, the confirmation of true co-crystal formation is difficult and tedious. Co-crystal confirmation typically requires complete characterization and comparison with all co-formers and their respective polymorphs. A 3:1 CL-20/TATB co-crystal was claimed based on the formation of unique peaks from PXRD and FTIR. However, a 2017 review by Wiscons and Matzger [16] evaluated several claimed energetic co-crystals and argued the peaks used to support the formation of a CL-20/TATB co-crystal are likely those of the hydrated α-CL-20 polymorph and not unique to co-crystal formation. This supported the claim that the reported CL-20/TATB crystal was more than likely a physical mixture [16]. However, the additional analysis by Wiscons and Matzger did not attempt to repeat the synthesis of CL-20/TATB due to the lack of procedural detail originally provided.

Therefore, the objective of this effort is two-fold. Firstly, investigate the preparation of a 3:1 CL-20/TATB co-crystal using the S/NS cocrystallization method with DMSO and water to provide confirmation or denial of the formation of a true co-crystal. If a true co-crystal cannot be claimed, then propose a solubility-based explanation of why TATB is not detected in the prepared material.

Secondly, assess the feasibility of forming a CL-20/TATB co-crystal using other solvent/nonsolvent combinations.

2 Experimental Section

2.1 Materials

CL-20, Class 1, (lot BAE13E051-164) was used. TATB was provided by Purdue University (lot BAE12K296-009). Dimethyl sulfoxide (DMSO), Ethyl Acetate, and Chloroform ACS grade were purchased from Fisher Scientific and used as recieved.

2.2 Synthesis

2.2.1 Neat Recrystallization

Complete characterization and confirmation of true co-crystal synthesis requires the comparison with neat components. It is common in the field of energetic co-crystals to compare co-crystal characterization data to that of neat components without taking into consideration interactions with the solvent or nonsolvent. Therefore, in this effort both CL-20 and TATB were recrystallized from DMSO using the same S/NS method. A physical mixture was also prepared from recrystallized neat components in a 3:1 molar ratio.

2.2.2 Co-crystal Synthesis

A 250 mg batch of 3:1 CL-20/TATB crystal was synthesized via S/NS crystallization. TATB was dissolved in 50 mL DMSO at 120 °C and stirred for one hour. CL-20 was then added to the solution and stirring was continued for several minutes. The solution was crashed with a 1:1 volumetric ratio of ice-cold deionized water. The solution was filtered using Whatman quantitative size 42 filter paper. Solids were collected and dried at 50 °C. A yield of 53.6 % was achieved. The prepared material will be subsequently referred to as **1**.

2.3 Characterization

DSC/TGA was carried out by a SDT Q600 Analyzer from TA instruments. A heating rate of 20 °C min^{-1} was used with UHP Argon flowing at 100 mL min^{-1}. Open alumina pans (90 μL) were used. All samples weighed between one and two mg and were heated from 50 to 600 °C. Data was analyzed using TA Universal Analysis software.

PXRD was performed using a Rigaku 500 diffractometer (Cu Kα radiation), with a tube voltage of 40 kV and tube current of 40 mA. Intensities were measured at double angle (2θ) values ranging from 7 to 50 degrees, at a speed of two degrees per minute. Data was processed in Jade v7.0 software.

SEM was carried out using a Zeiss Supra40VP variable-pressure field-emission scanning electron microscope at 10.00 kV. Samples were sputter coated with gold prior to imaging to reduce charging.

Raman spectroscopy was completed with a Foster and Freeman Foram X3 spectrometer using a 532 nm laser (power output of 8 mW). Multiple scan locations of each sample were averaged at a resolution of 2 cm^{-1}.

FTIR spectra were collected with a Nicolet iS10 FT-IR Spectrometer with the Smart ITX diamond ATR at resolution of 4 cm^{-1} through the IR range of 500–4000 cm^{-1}. Spectra were analyzed using OMNIC sotware.

3 Results and Discussion

3.1 Crystal Morphology

Crystal size and shape have been manipulated to tune the sensitivity and performance for energetic materials [17, 18]. Therefore, crystal morphology is one characterization technique for predicting sensitivity, performance, and co-crystal formation for energetic materials.

Crystal morphologies were evaluated using SEM and optical microscopy. Recrystallized TATB maintains its distinct yellow color with a smooth layered plate-like morphology. Each of the CL-20 polymorphs can be identified by their crystal morphology. Pure CL-20 phases have been reported to adopt several distinct morphologies. These morphologies
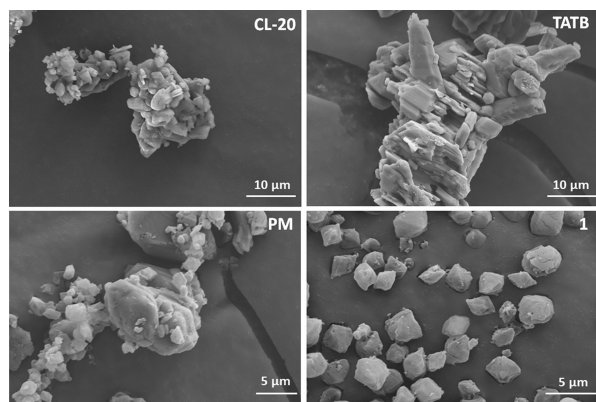
Figure 1. SEM imaging of CL-20, TATB, CL-20/TATB physical mixture (PM), and **1**.

Figure 2. DSC/TGA plots of CL-20/TATB materials. Neat components shown were those recrystallized from DMSO/Water.

include the α-phase as diamonds, β-phase as needles, and ε-phase as bipyramidal crystals [19, 20]. Recrystallization of CL-20 matches well with pure α-phase and confirms what has been reported for recrystallized α-CL-20 [18, 19]. SEM imaging shows that **1** adopts a unique crystal morphology when compared to the physical mixture of recrystallized components. No crystals resembling that of neat TATB were observed in **1** (Figure 1).

3.2 Thermal Properties

When a co-crystal is formed, the thermal properties indicated by the DSC curves are expected to be different than the pure components and that of the physical mixture. Co-crystals are formed from interactions and adopt a uniformity not found in physical mixtures of neat recrystallized components. These interactions could result in altered thermal behaviors detectable through DSC-TGA.

Differential scanning calorimetry data has shown that neat α-CL-20 exhibits an exothermic decomposition peak at 247.1 °C using a scan speed of 10 °C min^{-1} [21]. It can be seen in Figure 2 that CL-20 recrystallized from DMSO/Water exothermically decomposed at 247.44 °C resulting in negligible changes in thermal sensitivities compared with neat CL-20. Recrystallized TATB displayed an endothermic phase transition at 387 °C. Previously reported DSC data for TATB was for a N$_2$ atmosphere with an exothermic decomposition at 380.89 °C [12]. Differences between heat flow curves can be attributed to the use of crimped aluminum pans in the 2015 paper by Xu et al. versus open alumina pans used for this work [12].

The prepared physical mixture thermally decomposed at 232.13 °C, while **1** decomposed at a significantly higher temperature of 247.28 °C, similar to that of recrystallized CL-20. No attributable TATB peaks were observed in either the physical mixture or **1**. It was expected that the decomposition of CL-20 in both mixtures provided enough ther-
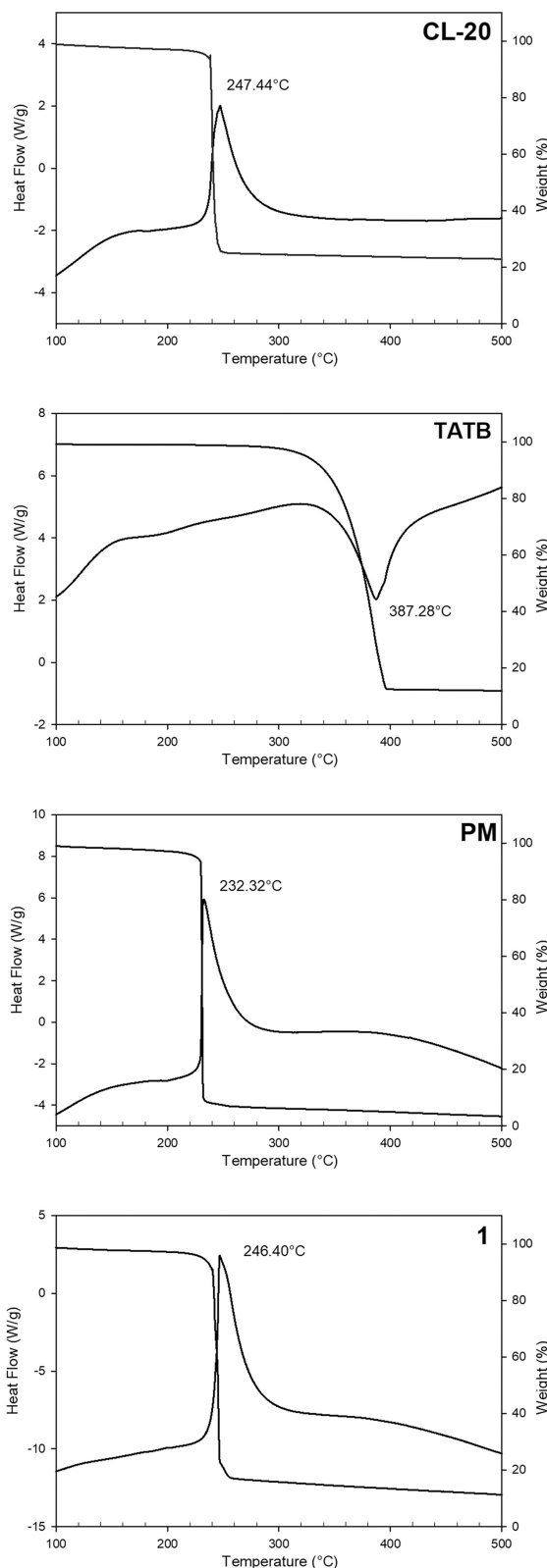
mal energy to decompose the TATB at a much lower temperature. Therefore, based on the observed thermal data it is expected that **1** may be a physical mixture and no noticeable differences in thermal stability were attributable to cocrystallization.

3.3 XRD

SC-XRD is preferred for analyzing the phases of cocrystallized materials; however, PXRD is used when crystal size does not meet the requirements for for SC-XRD. Relative peak intensities and peak positions are used to gain insight of the unit cell parameters, but are dependent on sample preparation methods, which are limited for energetic materials. It is important, but difficult, to assertain the differences between changes of unit cell composition and the changes of the crystal morphology of neat components [16]. The relatively small crystal diameter of **1**, approximately 2 μm, restricts the use SC-XRD analysis for **1.**

Recrystallized TATB had strong peaks at 28.23° and a doublet at 42.06° and 42.57° as shown in Figure 3. The prepared physical mixture displayed a strong TATB peak at 28.23° while **1** did not contain any detectable TATB peaks. This was the first indication that a true co-crystal was not formed. Recrystallized CL-20 exhibited strong peaks at 11.94° and 13.64° with a doublet at 27.39° and 27.81°. The PXRD pattern of **1** identified closely with that of recrystallized CL-20 with slight shifting of strong peaks to 11.76°, 13.43°, 27.21°, and 27.72° respectively. Peak intensities of **1** and the physical mixture were lower than that of the neat recrystallized components.
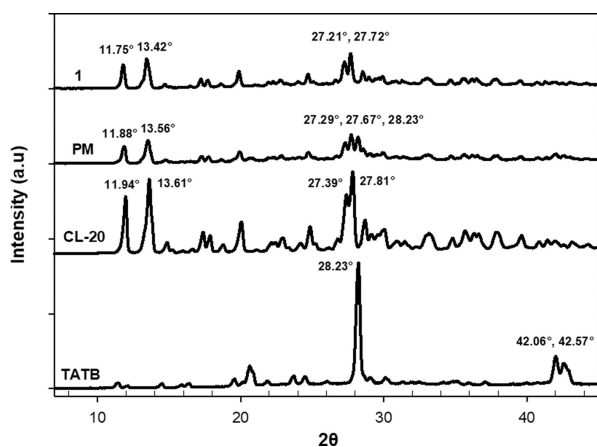

Figure 3. PXRD patterns for neat components, a physical mixture, and **1.**

3.4 FTIR and Raman Spectroscopy

FTIR and Raman spectroscopy are an invaluable characterization technique for the confirmation of true co-crystal formation. The analysis of vibrational frequencies can distinguish the intermolecular interactions that are present in both neat and cocrystalline materials. It is expected that a cocrystallized material would contain a combination of both single component spectra along with slight peak shifting [16]. Peak intensity changes should be noted as they are useful in identifying important stabilization forces. Due to their ability to detect different interactions, FTIR and Raman spectroscopy are used in coordination with each other to provide a powerful understanding of intermolecular interactions.

The Raman spectra of the prepared physical mixture and **1** are shown in Figure 4. All peaks of neat CL-20 and TATB were found in the physical mixture and **1**. Strong raman bands at 386 and 893 cm^{-1} in **1** indicate an increased ring deformation compared to recrystallized CL-20 and TATB [12]. The doublet observed at 386 cm^{-1} was also present as a strong peak in the physical mixture. The strong band at 846 cm^{-1} in recrystallized CL-20 and the physical mixture is unique to α-CL-20 but shifted to 852 cm^{-1} in **1**. An overlay of the physical mixture and **1** spectra showed similarities in peak intensity with band shifting of 5–10 wavenumbers.

Ghosh et al. [19] reported that α-CL-20 was distinguishable in FTIR spectroscopy by the presence of a low intensity hydrate peak at about 3700 cm^{-1} and a triplet-like feature near 745 cm^{-1} (739, 750, and 763 cm^{-1}). CL-20 recrystallized from DMSO/Water agreed well with the reported spectra and retained a sharp hydrate peak at 3693 cm^{-1} and a triplet at 739, 750, and 763 cm^{-1} found in Figure 5. The aforementioned α-CL-20 peaks were present in both the physical mixture and **1** without any distinguishable peak shifting.

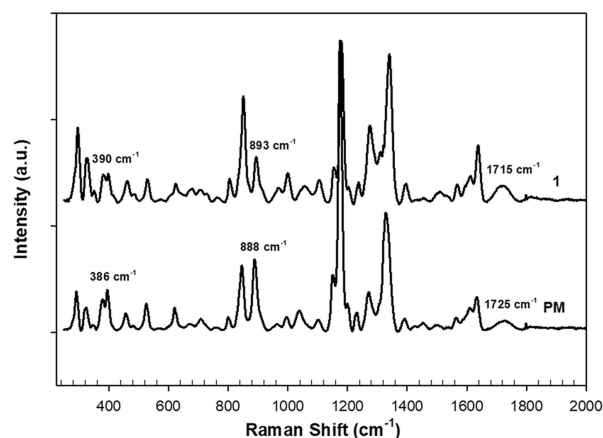Recrystallized TATB had strong peaks at 3307, 3206, 1436, 1208 cm^{-1}. Corresponding TATB peaks were weak

Figure 4. Comparison of the Raman spectra for a physical mixture and **1**.
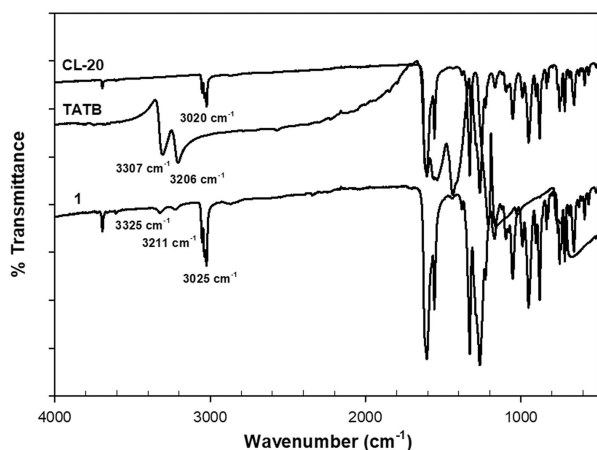
Figure 5. Comparison of the FTIR spectra for neat recrystallized components and **1**.
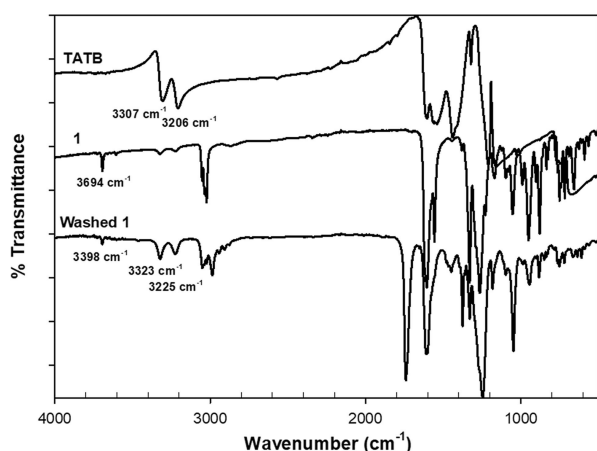

Figure 6. FTIR spectra for the washing of **1** with ethyl acetate.

Figure 7. SEM image comparison of **1** washed with ethyl acetate.

peaks in the physical mixture and barely distinguishable in **1** at 3325, 3211, and 1442 cm^{-1}.

The prepared co-crystal, **1**, maintained all α-CL-20 peaks with no detectable peak shifting. However, TATB peaks were much weaker than what would be expected for a 3:1 CL-20/TATB co-crystal.

3.5 Washing Experiments

The solubility of TATB significantly limited the possible synthesis routes of a CL-20/TATB co-crystal. The poor solubility of TATB in both DMSO and water should have led to the detection of TATB in **1**. The lack of TATB in **1** led to the exploration of possible explanations. Due to the natural desire to minimize the amount of solvent required, the mixture of CL-20 and TATB prior to the addition of nonsolvent was relatively close to the saturation point for TATB in DMSO. From a crystallization perspective, it was likely that TATB would
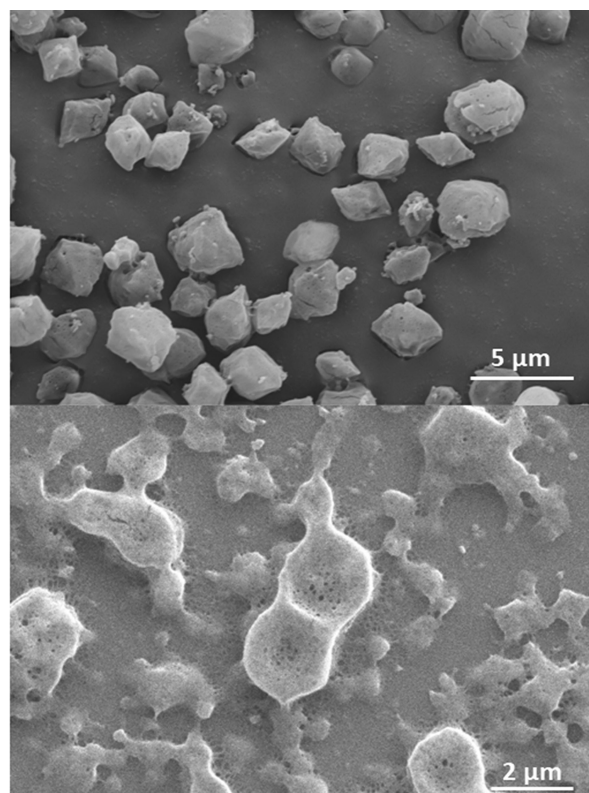
have been the first to precipitate during the addition of nonsolvent. A possible explanation would be that TATB acted as a nucleation site for CL-20 recrystallization and was difficult to detect during bulk characterization such as FTIR and XRD. To test this hypothesis, **1** was washed with ethyl acetate, an efficient solvent for CL-20, and the resulting material was again characterized via FTIR spectroscopy and SEM imaging.

The washed **1** material retained a weak α-CL-20 peak at 3692 cm^{-1} with the triplet becoming a doublet at 750 and 762 cm^{-1} as seen in Figure 6. A significant increase in TATB peak intensity was found when compared to non-washed **1** with shifting to 3323 and 3225 cm^{-1}. The increased intensity of TATB peaks post washing supported the idea that TATB is present in **1** but not at the defined stoichiometric ratio of 3:1.

SEM imaging of **1** post washing is found in Figure 7 and showed the washed material retained similar crystal morphology of **1**. The washed material also exhibited porosity not found in **1**.

3.6 Filtrate Characterization

The poor yield and the characterization of the washed **1** material led to the characterization of the DMSO/water filtrate. The filtrate was centrifuged, washed, and then dried.
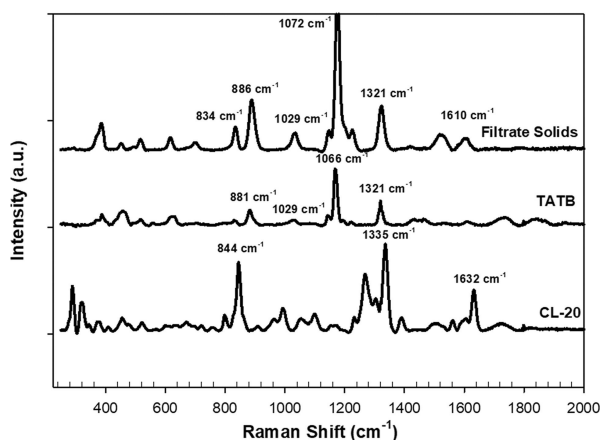
Figure 8. Raman spectra comparison of the filtrate solids leftover from the synthesis of **1**.
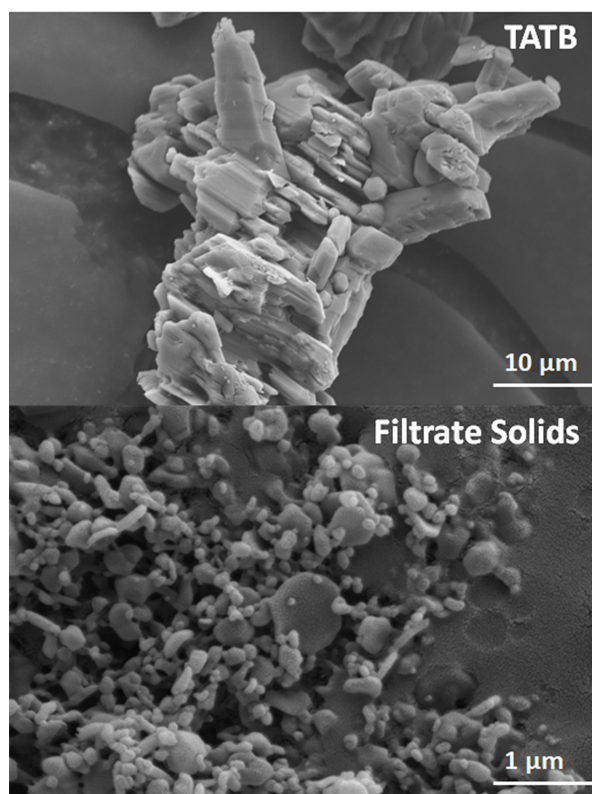

Figure 9. Comparison SEM micrographs of recrystallized TATB the solids found in the filtrate.

The filtrate solids were characterized via spectroscopy and SEM imaging.

FTIR confirmed the presence of TATB in the filtrate with strong peaks at 3318 and 3218 cm^{-1}. Overall, the FTIR spectra of filtrate solids matched closely with that of recrystallized TATB with peak shifts of 10–15 cm^{-1}. No unique CL-20

peaks were observed in the FTIR spectra, which is found in Figure 8, of the filtrate solids.

Raman spectra of the filtrate solids had possible TATB peaks at 886, 1029, 1072, and 1321 cm^{-1} with CL-20 peaks at 834 and 1321 cm^{-1}. The poor yield of the S/NS cocrystallization was likely due to TATB and CL-20 remaining in solution throughout the filtration process.

SEM imaging confirmed that TATB was adopting a morphology with a particle diameter on the nanoscale. This allowed TATB to easily pass through the Whatman quantitative size 42 filter paper which is rated to recover particles greater than 2.5 μm.

The adoption of this unique crystal morphology was not observed when neat TATB is crashed from DMSO with water. Therefore, the presence of CL-20 led to interactions that significantly impacted the morphology of TATB as shown in Figure 9.

Recent work exploring the cocrystallization mechanism of CL-20 and HMX suggests that crystallization propagates though secondary nucleation [22]. In secondary nucleation, cocrystallization takes place between tiny unstable nuclei that can be formed from a parent crystal or from the solution layer adjacent to the surface [23]. For the CL-20/HMX co-crystal mechanism, unstable nuclei, β-CL-20 and β-HMX, crystallize from solution first and cocrystallize together at a rate that is a function of suspension density. If CL-20/TATB followed a similar cocrystallization mechanism, the S/NS method with the instantaneous addition of NS used in this work does not allow for the individual components to achieve highly unstable nuclei concentrations like that of slow evaporation techniques.

3.7 Slow S/NS Cocrystallization

Due to the lack of S/NS procedural details reported for the original 2015 synthesis of CL-20/TATB, **1** was cocrystallized through the fast addition of NS to match the morphology of previously reported CL-20/TATB material. To investigate the potential dependence of true co-crystal formation on secondary nucleation, a second slow method was used where the addition of NS was carried out over 48 hours. (Procedure and characterization can be found in SI.1–SI.2) In short, **2** exhibited a unique crystal morphology compared to **1**. FTIR and PXRD analysis found that **2** exhibited TATB peaks that would be expected in a 3 : 1 co-crystal as compared to **1**, which lacked these significant TATB peaks. The yield of both fast and slow addition of NS was approximately the same at 53 % and analysis of the filtrate solids was performed. PXRD spectra of the filtrate solids, using the same methodology as was presented in section 3.6, found that slow addition of the NS resulted in predominately CL-20 in the filtrate, whereas the fast addition of NS resulted in a filtrate of predominately TATB. These experiments display the ability of manipulating the composition of the solid phase through NS addition rate. The rate of NS addition

should be carefully optimized for future S/NS cocrystallization methods, but still results in the likely formation a physical mixture regardless of rate for this particular system.

3.8 Polymorph Control of CL-20/TATB

The polymorphism of CL-20 can lead to large variances in performance and sensitivity [1, 14, 17, 24–26]. Several efforts have been made to investigate the effect of solvent choice on CL-20 polymorphism [17, 27]. In S/NS recrystallization and cocrystallization both the solvent and nonsolvent choices will dictate the morphology, sensitivity, and detonation properties of the resulting material. For example, the use of water as a nonsolvent will always result in the adoption of hydrated α-CL-20 polymorph, which has a less favorable sensitivity and detonation performance [20, 24, 28]. The relatively poor properties of α-CL-20, compared to that of other CL-20 polymorphs, demonstrates the need to explore other solvent combinations for the CL-20/TATB system.

The solubility of TATB requires that DMSO be used as the solvent. The only known solvents with "good" solubility at room temperature are superacids such as chlorosulfonic and highly concentrated sulfuric acid [29]. The selection of a nonsolvent can be modified. In hopes to produce a CL-20/TATB material with more favorable polymorphism, S/NS cocrystallization was attempted using DMSO and chloroform. Although CL-20 has exceptionally poor solubility in chloroform [30], a CL-20/TATB material was unable to be synthesized. Surprisingly, we observed no precipitation upon NS addition. We hypothesize that the interactions between CL-20 and DMSO led to an increased solubility of CL-20 in chloroform. The increased solubility limits the selection of standard nonsolvents, other than water, to control polymorphism, which always results in the hydrated polymorph. The solubility effects of DMSO on CL-20 should be considered for all future CL-20 based materials.

3.9 Future Exploration of CL-20/TATB Materials

Our attempts at forming CL-20 and TATB co-crystal have highlighted the presence of intermolecular interactions and their influence on crystal morphologies. These intermolecular interactions are often a good sign that formation of a co-crystal is possible under the right conditions but are not a guarantee of co-crystal formation. A thermodynamic approach of designing a more favorable cocrystallization synthesis method could be used in place of trial and error experimentation.

A 2015 paper by Wei et al. [31] assessed the thermodynamics behind the formation of energetic-energetic co-crystals. A variety of computational methods were employed to report the changes in Gibbs free energy and enthalpy of cocrystal formation. The authors report that the thermodynamic driving forces behind co-crystal formation are likely entropic rather than enthalpic [31]. They concluded that cocrystallization parameters such as solvent selection and adequate mixing are key factors in forming energetic cocrystals. While we do not have many alternatives for solvent selection for TATB, we can use the provided thermodynamic data to form conclusions regarding the effects of temperature. The enthalpy and Gibbs free energy of co-crystal formation for the CL-20-TATB system were used to solve for TΔS. We find that for a CL-20/TATB co-crystal in DMSO, the entropy change is negative, making higher temperatures *less* favorable for co-crystal formation.

These findings may explain why our attempts at producing a CL-20/TATB co-crystal have been unsuccessful. The limited solubility of TATB in DMSO led to the S/NS cocrystallization at 120 °C compared to 20 °C as reported in the 2015 paper. While cocrystallization at higher temperatures is beneficial for minimizing the amount of solvent required, it leads to less favorable thermodynamics for co-crystal formation. Ultimately, the lack of acceptable solvents and weak driving forces of co-crystal formation, make the synthesis of a true CL-20/TATB co-crystal highly unlikely.

4 Conclusions

The synthesis and confirmation of an energetic co-crystal is a difficult and tedious process. A 3:1 CL-20/TATB co-crystal was attempted via S/NS methods similar to those reported by Xu et al., in 2015. The adoption of a unique crystal morphology looked promising for the possibility of forming a novel energetic co-crystal. Further characterization of **1** highlighted the lack of TATB at the desired ratio.

S/NS cocrystallization of Cl-20/TATB with DMSO and water led to the formation of α-CL-20 and nanoscale TATB. Recrystallized TATB using the same solvent and nonsolvent procedure did not adopt the same morphology as found in the filtrate. These findings lead us to hypothesize that the presence of CL-20 results in intermolecular interactions with TATB that modify its crystal morphology. Washing experiments confirmed the presence of TATB within **1** detectable by FTIR spectroscopy. The lack of peak shifting, formation of unique peaks, and consistent distribution of TATB throughout the solid phase, support the conclusion that **1** identified more closely with that of a physical mixture than a true co-crystal. A thermodynamic analysis confirmed that higher cocrystallization temperatures resulted in less favorable energies for co-crystal formation. The thermodynamic driving forces and limited solubility limit the chances of forming a true CL-20/TATB co-crystal and should be considered for future co-crystal synthesis in general.

Symbols and Abbreviations

CL-20   Hexanitrohexaazaisowurtzitane
TNT   Trinitrotoluene

References

[1] D. I. Millar, H. E. Maynard-Casely, D. R. Allan, A. S. Cumming, A. R. Lennie, A. J. Mackay, I. D. Oswald, C. C. Tang, C. R. Pulham, Crystal engineering of energetic materials: Co-crystals of CL-20, *CrystEngComm* **2012**, *14*, 3742–3749.

[2] Y. A. Abramov, C. Loschen, A. Klamt, Rational coformer or solvent selection for pharmaceutical cocrystallization or desolvation, *J. Pharm. Sci.* **2012**, *101*, 3687–3697.

[3] O. Bolton, A. J. Matzger, Improved Stability and Smart-Material Functionality Realized in an Energetic Cocrystal, *Angew. Chem. Int. Ed.* **2011**, *50*, 8960–8963.

[4] O. Bolton, L. R. Simke, P. F. Pagoria, A. J. Matzger, High Power Explosive with Good Sensitivity: A 2:1 Cocrystal of CL-20:HMX, *Cryst. Growth Des.* **2012**, *12*, 4311–4314.

[5] Q. Cao, J. J. Xiao, P. Gao, S. S. Li, F. Zhao, Y. A. Wang, H. M. Xiao, Molecular dynamics simulations for CL-20/TNT co-crystal based polymer-bonded explosives, *J. Theor. Comput. Chem.* **2017**, *16*, 1750072.

[6] H. Gao, P. Du, X. Ke, J. Liu, G. Hao, T. Chen, W. Jiang, A Novel Method to Prepare Nano-sized CL-20/NQ Co-crystal: Vacuum Freeze Drying, *Propellants, Explos., Pyrotech.* **2017**, *42*, 889–895.

[7] H. Gao, W. Jiang, J. Liu, G. Hao, L. Xiao, X. Ke, T. Chen, Study of an Energetic-oxidant Co-crystal: Preparation, Characterisation, and Crystallisation Mechanism, *Def. Sci. J.* **2017**, *67*, 510–517.

[8] H. Gao, W. Jiang, J. Liu, G. Hao, L. Xiao, X. Ke, T. Chen, Synthesis and Characterization of a New Co-Crystal Explosive with High Energy and Good Sensitivity, *J. Energ. Mater.* **2017**, *35*, 490–498.

[9] G. Han, Q.-f. Li, R.-j. Gou, S.-h. Zhang, L. Wang, R. Guan, Growth morphology of CL-20/HMX cocrystal explosive: insights from solvent behavior under different temperatures, *J. Mol. Model.* **2017**, *23*, 360.

[10] H. Li, Y. Shu, S. Gao, L. Chen, Q. Ma, X. Ju, Easy methods to study the smart energetic TNT/CL-20 co-crystal, *J. Mol. Model.* **2013**, *19*, 4909–4917.

[11] U. Nair, R. Sivabalan, G. Gore, M. Geetha, S. Asthana, H. Singh, Hexanitrohexaazaisowurtzitane (CL-20) and CL-20-based formulations, *Combustion, Explosion, and Shock Waves* **2005**, *41*, 121–132.

[12] H. Xu, X. Duan, H. Li, C. Pei, A novel high-energetic and good-sensitive cocrystal composed of CL-20 and TATB by a rapid solvent/non-solvent method, *RSC Advances* **2015**, *5*, 95764–95770.

[13] C. Zhang, X. Xue, Y. Cao, J. Zhou, A. Zhang, H. Li, Y. Zhou, R. Xu, T. Gao, Toward low-sensitive and high-energetic co-crystal II:

[14] structural, electronic and energetic features of CL-20 polymorphs and the observed CL-20-based energetic-energetic cocrystals, *CrystEngComm* **2014**, *16*, 5905–5916.

[14] J. Zhang, Time for pairing: cocrystals as advanced energetic materials, *CrystEngComm* **2016**, *18*, 6124–6133.

[15] W. Zhang, J. Zhang, M. Deng, X. Qi, F. Nie, Q. Zhang, A promising high-energy-density material, *Nat. Commun.* **2017**, *8*, 181.

[16] R. A. Wiscons, A. J. Matzger, Evaluation of the Appropriate Use of Characterization Methods for Differentiation between Cocrystals and Physical Mixtures in the Context of Energetic Materials, *Cryst. Growth Des.* **2017**, *17*, 901–906.

[17] X. Jiang, X. Guo, H. Ren, Q. Jiao, Preparation and Characterization of Desensitized ε-HNIW in Solvent-Antisolvent Recrystallizations, *Cent. Eur. J. Energ. Mater.* **2012**, *9*, 219–236.

[18] A. Elbeih, A. Husarova, S. Zeman, Path to ε-HNIW with reduced impact sensitivity, *Cent. Eur. J. Energ. Mater.* **2011**, *8*, 173–182.

[19] M. Ghosh, V. Venkatesan, S. Mandave, S. Banerjee, N. Sikder, A. K. Sikder, B. Bhattacharya, Probing crystal growth of ε-and α-CL-20 polymorphs via metastable phase transition using microscopy and vibrational spectroscopy, *Cryst. Growth Des.* **2014**, *14*, 5053–5063.

[20] M. F. Foltz, C. L. Coon, F. Garcia, A. L. Nichols, The thermal stability of the polymorphs of hexanitrohexaazaisowurtzitane, Part I, *Propellants, Explos., Pyrotech.* **1994**, *19*, 19–25.

[21] M. F. Foltz, C. L. Coon, F. Garcia, A. L. Nichols, The thermal stability of the polymorphs of hexanitrohexaazaisowurtzitane, Part II, *Propellants, Explos., Pyrotech.* **1994**, *19*, 133–144.

[22] S. Sun, H. Zhang, Y. Liu, J. Xu, S. Huang, S. Wang, J. Sun, Transitions from Separately Crystallized CL-20 and HMX to CL-20/HMX Cocrystal Based on Solvent Media, *Cryst. Growth Des.* **2018**, *18*, 77–84.

[23] S. G. Agrawal, A. H. J. Paterson, Secondary Nucleation: Mechanisms and Models, *Chem. Eng. Commun.* **2015**, *202*, 698–706.

[24] J. Xu, Y. Tian, Y. Liu, H. Zhang, Y. Shu, J. Sun, Polymorphism in hexanitrohexaazaisowurtzitane crystallized from solution, *J. Cryst. Growth* **2012**, *354*, 13–19.

[25] Y. Bayat, V. Zeynali, Preparation and characterization of nano-CL-20 explosive, *J. Energ. Mater.* **2011**, *29*, 281–291.

[26] J. H. Urbelis, V. G. Young, J. A. Swift, Using solvent effects to guide the design of a CL-20 cocrystal, *CrystEngComm* **2015**, *17*, 1564–1568.

[27] M. Ghosh, V. Venkatesan, A. K. Sikder, N. Sikder, Preparation and Characterisation of [epsilon]-CL-20 by Solvent Evaporation and Precipitation Methods, *Def. Sci. J.* **2012**, *62*, 390.

[28] J.-H. Kim, Y.-C. Park, Y.-J. Yim, J.-S. Han, Crystallization Behavior of Hexanitrohexaazaisowurtzitane at 298 K and Quantitative Analysis of Mixtures of Its Polymorphs by FTIR, *J. Chem. Eng. Jpn.* **1998**, *31*, 478–481.

[29] M. F. Foltz, D. Ornellas, P. Pagoria, A. Mitchell, Recrystallization and solubility of 1,3,5-triamino-2,4,6-trinitrobenzene in dimethyl sulfoxide, *J. Mater. Sci.* **1996**, *31*, 1893–1901.

[30] P. Lv, H. Wang, Y. Tong, L. Dang, C. Sun, S.-P. Pang, Measurement and Correlation of the Solubility of ε-CL-20 in 12 Organic Solvents at Temperatures Ranging from 278.15 to 318.15 K, *J. Chem. Eng. Data* **2017**, *62*, 961–966.

[31] X. Wei, A. Zhang, Y. Ma, X. Xue, J. Zhou, Y. Zhu, C. Zhang, Toward low-sensitive and high-energetic cocrystal III: thermodynamics of energetic-energetic cocrystal formation, *CrystEngComm* **2015**, *17*, 9037–9047.